Helmholtz solitons in optical materials with a dual power-law refractive index

Christian, JM, McDonald, GS and Chamorro-Posada, P

http://dx.doi.org/10.1142/S0218863510005340

Helmholtz solitons in optical materials with a dual power-law refractive index

J. M. Christian and G. S. McDonald

Joule Physics Laboratory, School of Computing, Science and Engineering,

Materials & Physics Research Centre, University of Salford, Salford M5 4WT, U.K.

P. Chamorro-Posada

Departamento de Teoría de la Señal y Comunicaciones e Ingeniería Telemática, Universidad de Valladolid, ETSI Telecomunicación, Campus Miguel Delibes s/n, 47011 Valladolid, Spain

Submitted to *Journal of Nonlinear Optical Physics & Materials*

24th July 2010

Abstract

A nonlinear Helmholtz equation is proposed for modelling scalar optical beams in uniform planar waveguides whose nonlinear refractive index exhibits a purely-focusing dual power-law dependence on the electric field amplitude. Two families of exact analytical solitons, describing forward- and backward-propagating beams, are derived. These solutions are physically and mathematically distinct from those recently discovered for related nonlinearities. The geometry of the new solitons is examined, conservation laws are reported, and classic paraxial predictions are recovered in a simultaneous multiple limit. Conventional semi-analytical techniques assist in studying the stability of these nonparaxial solitons, whose propagation properties are investigated through extensive simulations.

PACS numbers: 42.65.–k (*nonlinear optics*), 42.65.Tg (*optical solitons*), 42.65.Wi (*nonlinear waveguides*), 05.45.Yv (*solitons*)

Keywords: Spatial solitons; Helmholtz diffraction; dual power-law materials.

1. Introduction

Spatial solitons are self-localizing self-stabilizing beams that can emerge as dominant modes in nonlinear systems. Optical spatial solitons are an important example, as they have been proposed to offer many applications within future technological systems.[1–3] The archetypal geometry for supporting spatial solitons is a two-dimensional (2D) uniform planar waveguide, which comprises a longitudinal direction and a single (effective) transverse direction. Such 2D solitons can be robust against perturbations, and for this reason they have been suggested as candidate optical bits in information communication and technology (ICT) devices.

Helmholtz soliton theory plays a key role in modelling a wide range of experimental contexts involving the oblique (off-axis) propagation of, and interaction between, continuous-wave broad scalar beams. Such considerations lie at the heart of multiplexing[4–6] and interface[7,8] scenarios. Paraxial angles of interaction, incidence, reflection, and refraction limit modelling to negligible or nearly-negligible magnitudes (with respect to the reference direction). Recently we have exploited exact analytical Helmholtz solitons to quantify, for the first time, the full range of angular characteristics of interaction[9] and interface[10–12] geometries.

In this paper, we consider spatial solitons in optical materials with a nonlinear refractive index $n_{NL}(E)$ whose dependence on the local electric field amplitude E is given by[13–17]

$$n_{NL}\left(E\right)=n_{\sigma}\left|E\right|^{\sigma}+n_{2\sigma}\left|E\right|^{2\sigma}. \tag{1}$$

Here, σ is a positive exponent and (n_{σ}, $n_{2\sigma}$) are real coefficients that can, potentially, assume either sign. Model (1) incorporates many different classes of scalar nonlinearities, including Kerr,[1–3] single power-law,[18,19] cubic-quintic,[20] and quadratic-cubic.[21] It also provides an approximation for a saturable refractive index.[22] Here, attention will be paid to the most general form of nonlinearity (i.e., arbitrary σ). Since a Helmholtz description of wave phenomena retains a more complete form of the Laplacian operator, this type of formulation may be considered as generic in character. Such a feature increases prospects that our results find application in other (non-optical) areas of nonlinear science.

Our previous studies have investigated two regimes where the self-lensing processes in model (1) are *competing* [i.e., where sgn($n_\sigma n_{2\sigma}$) = –1]. The case $n_\sigma > 0$, $n_{2\sigma} < 0$ supports bright solitons and a class of nonlinear boundary wave;[23] when $n_\sigma < 0$, $n_{2\sigma} > 0$, one finds coexisting bright hyperbolic solitons, algebraic (bright and dark) solitons, and also class of nonlinear periodic wave.[24] The stability properties of those various solutions have been characterized by semi-analytical and computational investigations. For completeness, we now explore the remaining scenario that can be expected to support bright solitons: the *purely focusing* nonlinearity, where $n_\sigma > 0$ and $n_{2\sigma} > 0$.

In Section 2 of this paper, the dual power-law Helmholtz model is presented and its spatial symmetry properties are discussed. Two families of exact analytical bright soliton solution, describing forward and backward stationary beams, are then derived and their geometry is explored in detail. These solitons are distinct from those in competitive-focusing regimes. Three conservation laws for the dual power-law Helmholtz equation are given in both general (integral) and particular (algebraic) forms. An asymptotic analysis reveals that the forward solutions and their associated invariants converge to their paraxial counterparts. However, no such convergence is uncovered for backward solutions, which is entirely consistent with the uni-directionality of conventional (paraxial) frameworks. In Section 3, exhaustive computer simulations investigate the robustness of the new solitons against perturbations to the beam shape, and regions of stability in the solution parameter space are mapped out. We conclude, in Section 4, with some comments about the significance and potential applicability of our results.

2. Helmholtz Soliton Theory

2.1. *Model equations and spatial symmetry*

We consider a transverse-electric (TE polarized) scalar electric field

$$\tilde{E}(x,z,t) = E(x,z)\exp(-i\omega t) + E^*(x,z)\exp(+i\omega t), \tag{2}$$

where (x, z) and t are the laboratory space and time coordinates, respectively, and ω is the optical carrier frequency. The spatial part of the electric field, $E(x,z)$, then satisfies the Helmholtz equation[25–28]

$$\left(\frac{\partial^2}{\partial z^2}+\frac{\partial^2}{\partial x^2}\right)E(x,z)+\frac{\omega^2}{c^2}n^2(E)E(x,z)=0\,, \tag{3}$$

where c is the (vacuum) speed of light and the dielectric properties of the medium are described within the function n^2. In uniform media, there is no physical distinction between the transverse and longitudinal directions. This spatial symmetry appears in Eq. (3) as the invariance of the in-plane Laplacian $\partial_{zz}+\partial_{xx}$ under arbitrary rotations of the coordinate axes through angle θ (see Fig. 1). Bi-directionality is another key property of Eq. (2), and one subsequently expects to find both forward- and backward-travelling waves. Counterpropagation soliton solutions are also possible.[29]

A weakly-nonlinear refractive index $n(E) = n_0 + n_{NL}(E)$ is well described by $n^2(E) \simeq n_0^2 + 2n_0 n_{NL}(E)$, where n_0 is the linear index (at frequency ω). For the dual power-law nonlinearity, this approximation requires n_0 to be much larger than both $n_\sigma E_0{}^\sigma$ and $n_{2\sigma} E_0{}^{2\sigma}$, where E_0 is the peak amplitude of the field. By introducing model (1) and writing $E(x,z) = E_0 u(x,z)\exp(ikz)$, where z is taken to be the reference (longitudinal) direction, a dimensionless equation for the complex envelope u can be derived without further approximation:[23,24]

$$\kappa\frac{\partial^2 u}{\partial\zeta^2}+i\frac{\partial u}{\partial\zeta}+\frac{1}{2}\frac{\partial^2 u}{\partial\xi^2}+\alpha|u|^\sigma u+\gamma|u|^{2\sigma}u=0\,. \tag{4}$$

Here, $\zeta = z/L_D$ and $\xi = 2^{1/2}x/w_0$, where $L_D = kw_0{}^2/2$ is the diffraction length of a reference (paraxial) Gaussian beam, $k = n_0 k_0$ is the wavenumber of the carrier wave, and $k_0 = \omega/c = 2\pi/\lambda$. The inverse beam-width is quantified by $\kappa \equiv 1/(kw_0)^2 = \varepsilon^2/4\pi^2 n_0{}^2$, where $\varepsilon \equiv \lambda/w_0$. Throughout this paper, it is assumed that $\lambda << w_0$ so that $\kappa \sim \varepsilon^2 << O(1)$, which is a requirement for the validity of scalar Helmholtz modelling. Finally, the parameters α and γ are related to the (real) scale factor E_0. Since we are interested in the purely-focusing nonlinearity (where $n_\sigma > 0$ and $n_{2\sigma} > 0$), a convenient normalization might be $E_0 \equiv$

$(n_0/n_\sigma L_D k)^{1/\sigma}$, so that $\alpha = 1$ and $\gamma = E_0{}^\sigma(n_{2\sigma}/n_\sigma)$. For maximum generality, α and γ will be kept as independent (positive) parameters for now.

Ultranarrow-beam effects are unimportant in contexts where $\varepsilon << O(1)$; they come into play when the beam waist and free-space wavelength are comparable [i.e., where $\varepsilon = O(1)$] and describe, for example, the miniaturization aspects of ICT applications (where the physical dimensions of a device may approach optical-wavelength scales). Broad-beam geometries avoid such involved field descriptions, where one must take full account of the $\nabla(\nabla\cdot\mathbf{E})$ term in Maxwell's equations.[30–33]

2.2. *Exact analytical bright solitons*

We now present a thorough derivation of the exact analytical bright solitons of Eq. (4). One begins by seeking solutions that have the form $u(\xi,\zeta) = F(\xi,\zeta)\exp[i(K_\xi\xi + K_\zeta\zeta)]\exp(-i\zeta/2\kappa)$. This representation splits the field u into a (real) envelope function $F(\xi,\zeta)$ (that describes the spatial profile of a beam) and a travelling-wave part with (normalized) wavevector $\mathbf{K} = (K_\xi, K_\zeta)$. By substituting the expression for u into the governing equation, one obtains two coupled partial differential equations for F,

$$\kappa\frac{\partial^2 F}{\partial\zeta^2} + \frac{1}{2}\frac{\partial^2 F}{\partial\xi^2} - \beta F + \alpha F^{\sigma+1} + \gamma F^{2\sigma+1} = 0\,, \tag{5a}$$

$$2\kappa K_\zeta\frac{\partial F}{\partial\zeta} + K_\xi\frac{\partial F}{\partial\xi} = 0\,, \tag{5b}$$

where the real parameter β has been introduced through

$$\kappa K_\zeta^2 - \frac{1}{4\kappa} + \frac{1}{2}K_\xi^2 \equiv \beta\,. \tag{5c}$$

A more detailed description of the role played by β will be presented shortly; it is particularly important in the context of analysing soliton stability problems. Equation (5*c*) is an elliptic dispersion relation, reflecting the fact that Helmholtz wave equations generally support propagation in both forward and backward directions.[28] One now introduces the new variable $s = (\xi + V\zeta)/(1 + 2\kappa V^2)^{1/2}$ which is the coordinate perpendicular to the beam's propagation

axis. By implementing this transformation, which is parameterized by the conventional transverse velocity V,[28] Eqs. (5*a*) and (5*b*) simplify to

$$\frac{1}{2}\frac{d^2F}{ds^2} - \beta F + \alpha F^{\sigma+1} + \gamma F^{2\sigma+1} = 0\,, \tag{6a}$$

$$\left(K_\xi + 2\kappa V K_\zeta\right)\frac{dF}{ds} = 0\,. \tag{6b}$$

To derive particular solutions (i.e., bright solitons), Eqs. (6*a*) and (6*b*) must be supplemented by appropriate boundary conditions. These are typically

$$\lim_{s\to 0} F(s) \to \text{const.}\,, \quad \lim_{s\to\pm\infty} F(s) \to 0\,, \quad \lim_{s\to 0}\frac{dF(s)}{ds} \to 0\,, \quad \lim_{s\to\pm\infty}\frac{dF(s)}{ds} \to 0\,. \tag{7a,b,c,d}$$

Since the derivative dF/ds is non-zero [except at certain limiting points in s – refer to Eqs. (7*c*) and (7*d*)], the only consistent solution to Eq. (6*b*) is $K_\xi = -2\kappa V K_\zeta$. By eliminating K_ξ^2 from Eq. (5*c*), it can be shown that

$$K_\zeta = \pm\frac{1}{2\kappa}\sqrt{\frac{1+4\kappa\beta}{1+2\kappa V^2}}\,. \tag{8}$$

Here, the $\pm$ sign illustrates that the longitudinal projection of the soliton wavevector **K** can have a component along either the forward (+) or backward (–) longitudinal direction. The integration of Eq. (6*a*) is simplified by introducing the substitution $F(s) = f^{1/\sigma}(s)$, and solving instead for f.[13] When this procedure is completed, one is left with the exact analytical soliton of Eq. (4):

$$\begin{aligned} u(\xi,\zeta) = \eta\Bigg[A\cosh\left(\sigma\sqrt{2\beta}\,\frac{\xi + V\zeta}{\sqrt{1+2\kappa V^2}}\right) + 1\Bigg]^{-1/\sigma} \\ \times \exp\left[\pm i\sqrt{\frac{1+4\kappa\beta}{1+2\kappa V^2}}\left(-V\xi + \frac{\zeta}{2\kappa}\right)\right]\exp\left(-i\frac{\zeta}{2\kappa}\right), \end{aligned} \tag{9a}$$

where

$$A \equiv \left[1 + \frac{(2+\sigma)^2}{1+\sigma}\left(\frac{\gamma}{\alpha^2}\right)\beta\right]^{1/2} \quad \text{and} \quad \eta \equiv \left(\frac{2+\sigma}{\alpha}\beta\right)^{1/\sigma}. \tag{9b,c}$$

This solution describes an exponentially localized stationary beam with peak amplitude $\eta/(A + 1)^{1/\sigma}$ and transverse velocity V.

For clarity, it is worth pointing out the differences between the new Helmholtz soliton (9) and those solutions derived in our two earlier studies (for competing nonlinearities). On the one hand, parameters A and η in Eqs. (9*b*) and (9*c*) have the same formal structure as those in Ref. 24 (where $n_\sigma < 0$, $n_{2\sigma} > 0$) but, here, the envelope $[...]^{-1/\sigma}$ involves a "+1" term instead of a "– 1". This distinction means that for the purely-focusing nonlinearity, the limit $\beta \to 0$ describes a beam whose peak amplitude tends to zero (compare this to Ref. 24, where a non-vanishing peak amplitude in the same limit led to algebraic solitons). On the other hand, solution (9*a*) is formally identical to that in Ref. 23 (where $n_\sigma > 0$, $n_{2\sigma} < 0$), but the parameter A in Eq. (9*b*) is different here.

2.3. *Off-axis evolution and symmetric representations*

The conventional transverse velocity parameter V is related to the propagation angle θ of the beam in the laboratory (x, z) frame through[28]

$$\tan\theta = \sqrt{2\kappa}V\,, \tag{10}$$

where $-\infty \le V \le +\infty$ corresponds to $-90° \le \theta \le +90°$. The lower sign in solution (9*a*) represents a similar beam propagating in the opposite direction (refer to Fig. 1). By deploying the trigonometric identities[28] $\cos\theta = 1/(1+2\kappa V^2)^{1/2}$ and $\sin\theta = (2\kappa)^{1/2}V/(1+2\kappa V^2)^{1/2}$, one can combine the two solutions in (9*a*) into a single beam that propagates at angle $-180° \le \theta \le +180°$ with respect to the $+z$ direction:

$$\begin{aligned} u(\xi,\zeta) = \eta\left\{A\cosh\left[\sigma\sqrt{2\beta}\left(\xi\cos\theta + \frac{\zeta}{\sqrt{2\kappa}}\sin\theta\right)\right] + 1\right\}^{-1/\sigma} \\ \times \exp\left[i\sqrt{\frac{1+4\kappa\beta}{2\kappa}}\left(-\xi\sin\theta + \frac{\zeta}{\sqrt{2\kappa}}\cos\theta\right)\right]\exp\left(-i\frac{\zeta}{2\kappa}\right). \end{aligned} \tag{11}$$

Solution (11) reveals the implicit symmetry between "forward" and "backward" beams.[9,28]

A single beam propagating obliquely at angle θ in the (x, z) frame acquires a transverse velocity V in the (ξ, ζ) frame. An observer in the (x, z) frame then perceives the beam width to be increased, through geometrical projection, by a factor of $(1+2\kappa V^2)^{1/2} = \sec\theta$ (see Fig. 2). For moderate angles such as $|\theta| = 60°$ one has that $\sec\theta = 2$, *irrespective* of both κ and the system nonlinearity. The projected width has thus doubled relative to its on-axis value.[34] We stress that such broadening is not of purely geometrical significance. In fundamental optical geometries, such as nonlinear beam interactions and soliton refraction, this broadening can lead to corrections to paraxial predictions exceeding 100%, and even give rise to new regimes of behaviour.[9–12] In the limiting cases of $\theta = \pm 90°$, solution (11) becomes

$$u(\xi,\zeta) = \eta\left[A\cosh\left(\sigma\sqrt{2\beta}\,\frac{\zeta}{\sqrt{2\kappa}}\right)+1\right]^{-1/\sigma}\exp\left(\mp i\sqrt{\frac{1+4\kappa\beta}{2\kappa}}\,\xi\right)\exp\left(-i\frac{\zeta}{2\kappa}\right). \qquad (12)$$

This beam is localized in z but infinitely broad in x since propagation takes place perpendicularly to the reference direction.

2.4. *Conservation laws*

Model (4) and its complex-conjugate are conservative nonintegrable systems that can be treated as the Euler-Lagrange equations,

$$\frac{\not\partial \mathcal{L}}{\not\partial u^*} \equiv \frac{\partial \mathcal{L}}{\partial u^*} - \frac{\partial}{\partial\zeta}\left(\frac{\partial \mathcal{L}}{\partial u^*_\zeta}\right) - \frac{\partial}{\partial\xi}\left(\frac{\partial \mathcal{L}}{\partial u^*_\xi}\right) = 0 \quad \text{and} \quad \frac{\not\partial \mathcal{L}}{\not\partial u} \equiv \frac{\partial \mathcal{L}}{\partial u} - \frac{\partial}{\partial\zeta}\left(\frac{\partial \mathcal{L}}{\partial u_\zeta}\right) - \frac{\partial}{\partial\xi}\left(\frac{\partial \mathcal{L}}{\partial u_\xi}\right) = 0\,, \qquad (13a,b)$$

respectively, for a Lagrangian density $\mathcal{L}$, where $u_\zeta \equiv \partial u/\partial\zeta$ etc., and

$$\mathcal{L} = \frac{i}{2}\left(u^*\frac{\partial u}{\partial\zeta} - u\frac{\partial u^*}{\partial\zeta}\right) - \kappa\frac{\partial u}{\partial\zeta}\frac{\partial u^*}{\partial\zeta} - \frac{1}{2}\frac{\partial u}{\partial\xi}\frac{\partial u^*}{\partial\xi} + \alpha\frac{|u|^{2+\sigma}}{1+\frac{1}{2}\sigma} + \gamma\frac{|u|^{2(1+\sigma)}}{1+\sigma}\,. \qquad (14)$$

The canonically-conjugate momentum variables are

$$\pi \equiv \frac{\partial \mathcal{L}}{\partial u_\zeta} = \left(\frac{i}{2} - \kappa\frac{\partial}{\partial\zeta}\right)u^* \quad \text{and} \quad \tilde{\pi} \equiv \frac{\partial \mathcal{L}}{\partial u^*_\zeta} = -\left(\frac{i}{2} + \kappa\frac{\partial}{\partial\zeta}\right)u\,, \qquad (15a,b)$$

where $\pi = \tilde{\pi}^*$ since $\mathcal{L}$ has been constructed to be real. By exploiting standard field-theoretic techniques,[35] one can arrive at three fundamental conservation laws:

$$\frac{dW}{d\zeta} = \frac{d}{d\zeta}\int_{-\infty}^{+\infty} d\xi \left(\pi\delta u + \tilde{\pi}\delta u^*\right) = 0\,, \tag{16a}$$

$$\frac{dM}{d\zeta} = \frac{d}{d\zeta}\int_{-\infty}^{+\infty} d\xi \left(\pi\frac{\partial u}{\partial \xi} + \tilde{\pi}\frac{\partial u^*}{\partial \xi}\right) = 0\,, \tag{16b}$$

$$\frac{dH}{d\zeta} = \frac{d}{d\zeta}\int_{-\infty}^{+\infty} d\xi \left(\pi\frac{\partial u}{\partial \zeta} + \tilde{\pi}\frac{\partial u^*}{\partial \zeta} - \mathcal{L}\right) = 0\,. \tag{16c}$$

The origin of these conserved quantities lies in the invariance of the Euler-Lagrange equations (13a) and (13b) under a set of continuous one-parameter transformations: a global phase change [i.e., $u \rightarrow u' = \exp(\mathrm{i}\rho)u \simeq (1 + \mathrm{i}\rho)u \equiv u + \delta u$, where ρ is a real constant, $\delta u = \mathrm{i}\rho u$ and $\delta u^* = -\mathrm{i}\rho u^*$], and infinitesimal translations in ξ and ζ, respectively. By substituting Eqs. (15a) and (15b) into Eqs. (16a)–(16c), one can derive integral expressions for the energy-flow W, the momentum M, and the Hamiltonian H:

$$W = \int_{-\infty}^{+\infty} d\xi \left[|u|^2 - \mathrm{i}\kappa\left(u^*\frac{\partial u}{\partial \zeta} - u\frac{\partial u^*}{\partial \zeta}\right)\right], \tag{17a}$$

$$M = \int_{-\infty}^{+\infty} d\xi \left[\frac{\mathrm{i}}{2}\left(u^*\frac{\partial u}{\partial \xi} - u\frac{\partial u^*}{\partial \xi}\right) - \kappa\left(\frac{\partial u^*}{\partial \zeta}\frac{\partial u}{\partial \xi} + \frac{\partial u^*}{\partial \xi}\frac{\partial u}{\partial \zeta}\right)\right], \tag{17b}$$

$$H = \int_{-\infty}^{+\infty} d\xi \left[\frac{1}{2}\frac{\partial u^*}{\partial \xi}\frac{\partial u}{\partial \xi} - \kappa\frac{\partial u^*}{\partial \zeta}\frac{\partial u}{\partial \zeta} - \alpha\frac{|u|^{2+\sigma}}{1+\frac{1}{2}\sigma} - \gamma\frac{|u|^{2(1+\sigma)}}{1+\sigma}\right]. \tag{17c}$$

By expressing soliton (9) in the form $u(\xi,\zeta) = F(s)\exp[i(K_\xi\xi + K_\zeta\zeta)]\exp(-i\zeta/2\kappa)$, and substituting into Eqs. (17a)–(17c), a set of compact algebraic expressions for the three invariants can be obtained:

$$W = \pm\left(1 + 4\kappa\beta\right)^{1/2} P\,, \tag{18a}$$

$$M = \frac{V}{\sqrt{1 + 2\kappa V^2}}\left[\left(1 + 4\kappa\beta\right)P - 2\kappa Q\right], \tag{18b}$$

$$H = \frac{W}{2\kappa} - \frac{1}{\sqrt{1+2\kappa V^2}}\left(\frac{1}{2\kappa}\right)\left[\left(1+4\kappa\beta\right)P - 2\kappa Q\right]. \tag{18c}$$

The quantities $P \equiv P(\beta;\alpha,\gamma,\sigma)$ and $Q \equiv Q(\beta;\alpha,\gamma,\sigma)$ are given by the integrals

$$P \equiv \int_{-\infty}^{+\infty} ds\ F^2(s) = \frac{2}{\sqrt{2\beta}}\left(\frac{\eta^2}{\sigma}\right)\int_0^{+\infty} dy\ \left[A\cosh(y)+1\right]^{-2/\sigma} \tag{18d}$$

$$Q \equiv \int_{-\infty}^{+\infty} ds\ \left[\frac{d}{ds}F(s)\right]^2 = 2\sqrt{2\beta}\left(\frac{\eta^2 A^2}{\sigma}\right)\int_0^{+\infty} dy\ \sinh^2(y)\left[A\cosh(y)+1\right]^{-(2+2/\sigma)}. \tag{18e}$$

The integrals in Eqs. (18*d*) and (18*e*) can be evaluated analytically in the particular cases of $\sigma = 1$ and $\sigma = 2$ (they involve elementary functions, such as "$\tan^{-1}$"). In the next sub-section, it will be seen that P is formally identical to the integrated beam power of the corresponding paraxial soliton.[13] We also mention the interesting point that Helmholtz solitons satisfy the free-particle energy-momentum relationship $\partial H/\partial M = \partial_V H/\partial_V M = V$, where $\partial_V \equiv \partial/\partial V$.

2.5. *The paraxial approximation*

The arbitrary magnitude of the correction term $2\kappa V^2$ indicates that the operator $\kappa\partial_{\zeta\zeta}$ cannot generally be interpreted as a small [e.g., $O(\kappa)$] perturbation to an underlying paraxial governing equation. A rigorous recovery of the paraxial model demands that all contributions from $\kappa\partial_{\zeta\zeta}$ are negligible *simultaneously*. Conversely, if only one of these simultaneous conditions is not met, then a Helmholtz description is necessary. It is instructive to apply the multiple limit $\kappa \to 0$ (broad beam), $\kappa\beta \to 0$ (moderate intensity), and $\kappa V^2 \to 0$ (negligible propagation angle) to solution (9*a*). To leading order in these corrections,

$$\begin{aligned} u(\xi,\zeta) = \eta\left\{A\cosh\left[\sigma\sqrt{2\beta}\left(1-\kappa V^2\right)\left(\xi+V\zeta\right)\right]+1\right\}^{-1/\sigma} \\ \times\exp\left\{\mp iV\left(1-\kappa V^2+2\kappa\beta\right)\xi \pm i\left[\beta\left(1-\kappa\beta-\kappa V^2\right)-\frac{V^2}{2}\left(1-\frac{3}{2}\kappa V^2\right)\right]\zeta\right\} \\ \times\exp\left[-i\left(1\mp 1\right)\frac{\zeta}{2\kappa}\right]. \end{aligned} \tag{19}$$

In regimes where $\beta \leq O(1)$ and $|V| \leq O(1)$, the forward Helmholtz beam converges to the paraxial soliton of Micallef *et al.*,[13] namely

$$u(\xi,\zeta) \sim \eta \left\{ A\cosh\left[\sigma\sqrt{2\beta}\left(\xi + V\zeta\right)\right] + 1 \right\}^{-1/\sigma} \exp\left[-iV\xi + i\left(\beta - \frac{V^2}{2} \right)\zeta \right]. \qquad (20)$$

From this result, it can be seen that the β parameter in the forward Helmholtz soliton can be identified with the longitudinal phase shift of the corresponding paraxial solution. On the other hand, the backward Helmholtz beam tends to

$$u(\xi,\zeta) \sim \eta \left\{ A\cosh\left[\sigma\sqrt{2\beta}\left(\xi + V\zeta\right)\right] + 1 \right\}^{-1/\sigma} \exp\left[+iV\xi - i\left(\beta - \frac{V^2}{2} \right)\zeta \right] \exp\left(-i2\frac{\zeta}{2\kappa} \right), \quad (21)$$

which retains a κ-dependent rapid phase contribution. There is no analogue of this solution in paraxial theory, and its absence confirms that such models describe waves travelling in a single longitudinal direction only. The same multiple-limit procedure can also be applied to the invariants (18*a*)–(18*c*). To leading order,

$$W = \pm\left(1 + 2\kappa\beta\right)P, \qquad (22a)$$

$$M = V\left[\left(1 + 4\kappa\beta - \kappa V^2\right)P - 2\kappa Q \right], \qquad (22b)$$

$$H = \left(1 + 4\kappa\beta - \frac{3}{2}\kappa V^2 \right)\frac{1}{2}V^2 P - \left(2 \mp 1 \pm \kappa\beta\right)\beta P + \left(1 - \kappa V^2\right)Q - \left(1 \mp 1\right)\frac{P}{2\kappa}. \qquad (22c)$$

The conserved quantities of the forward beam converge to their paraxial counterparts,[16] $W \sim P$, $M \sim VP$, and $H \sim \frac{1}{2}V^2P - \beta P + Q$. The quantity P defined in Eq. (18*d*) may thus be interpreted as the integrated power of the corresponding paraxial soliton in Eq. (20). Similarly, the conserved quantities for the backward beam tend to $W \sim -P$, $M \sim VP$, and $H \sim \frac{1}{2}V^2P - 3\beta P + Q - P/\kappa$. Negative energy-flows do not appear in paraxial theory [since the integrand in Eq. (18*d*) is always positive-definite], and the Hamiltonian diverges as κ^{-1}. These results demonstrate that the paraxial approximation is much more subtle than simply $\kappa \simeq 0$, and that $\kappa \to 0$ is a necessary but not sufficient condition for the validity of paraxial models.

3. Stability of Helmholtz Solitons

3.1. *Stability criterion*

Soliton stability problems in paraxial (i.e., NLS-type) models are frequently addressed using the well-known Vakhitov-Kolokolov integral criterion.[36,37] Solution (20) can be stable against small perturbations provided the inequality

$$\frac{dP}{d\beta} \equiv \frac{d}{d\beta} \int_{-\infty}^{+\infty} d\xi \ \left| u(\xi, \zeta; \beta) \right|^2 > 0 \tag{23}$$

is satisfied,[13,14] where P is the integrated beam power [whose specific form is given in Eq. (18*d*)] and β is the wavenumber. The VK criterion can be used to map the regions of parameter space where solution (20) can be stable (see Fig. 3). We note that the VK criterion only considers linearized (i.e., small) perturbations. Furthermore, it only provides a necessary (not sufficient) condition for stability. The criterion is thus used to provide analytical stability boundaries which we subsequently test with rigorous (i.e., fully-nonlinear) simulations.

Without loss of generality, we set $\alpha = \gamma = +1$ throughout this analysis. When $0 < \sigma \leq 2$, the power $P(\beta)$ increases monotonically with β. Since $dP/d\beta > 0$ is always met, solitons in this region are predicted to be unconditionally stable. The situation changes when $2 < \sigma < 4$. There, $P(\beta)$ initially increases but eventually passes through a (σ-dependent) local maximum (β_{max}, P_{max}) after which $dP/d\beta < 0$. Solitons in this σ domain can be stable provided $\beta < \beta_{max}$, where β_{max} must be determined numerically. Solutions with $\sigma \geq 4$ are always unstable since $dP/d\beta < 0$. We note that the $P(\beta)$ characteristics for the purely-focusing nonlinearity (shown in Fig. 3) are distinct from their competitive-focusing counterparts.[23,24]

Previously, the VK criterion has been successfully deployed in the analysis of Helmholtz solitons.[23,24,38,39] The validity of this approach lies in spatial symmetry (see Fig. 4), where one expects the Helmholtz solutions (9) to be stable in the same regions of parameter space as their paraxial counterparts. On-axis forward beams (where $V = \kappa V^2 = 0$) with $\kappa << O(1)$ and $\beta \leq O(1)$ are quasi-paraxial; they are identical to their paraxial counterparts except for an $O(\kappa\beta)$ correction to the phase shift; from Eq. (19),

$$u(\xi,\zeta) \simeq \eta\left[A\cosh\left(\sigma\sqrt{2\beta}\xi\right)+1\right]^{-1/\sigma}\exp\left[i\beta\left(1-\kappa\beta\right)\zeta\right]. \qquad (24)$$

If the paraxial soliton (which naturally has $\kappa\beta = 0$) is stable [i.e., satisfies inequality (23)], then one also anticipates the quasi-paraxial Helmholtz soliton (24) to be stable (since the leading-order correction is negligibly small). For a single isolated beam, oblique evolution can be eliminated by a rotation of the observer's coordinate axes. Mathematically, one should ideally be able to describe the beam from *any* frame of reference, and transformations between different frames must leave its physical properties unchanged. If the on-axis beam is stable, then off-axis propagation in uniform media cannot give rise to instability.

3.2. *Numerical perturbation analysis*

The stability of Helmholtz soliton (9) against local perturbations to its shape can be studied numerically.[40] We focus our attention to input beams of the form[34]

$$u(\xi,0) = \eta\left[A\cosh\left(\sigma\sqrt{2\beta}\xi\right)+1\right]^{-1/\sigma}\exp\left(-iV\sqrt{\frac{1+4\kappa\beta}{1+2\kappa V^2}}\xi\right), \qquad (25)$$

whose launching angle, from Eq. (10), is $\theta = \tan^{-1}[(2\kappa)^{1/2}V]$. The perturbation arises from omission of the geometrical broadening factor in the amplitude profile. Initial condition (25) is then formally identical to an exact paraxial solution (20) with transverse velocity $S = V[(1 + 4\kappa\beta)/(1 + 2\kappa V^2)]^{1/2} = [(1 + 4\kappa\beta)/2\kappa]^{1/2}\sin\theta$. The initial-value problem can thus be interpreted as considering the effect of launching paraxial solitons into off-axis regimes when one does not make full allowance for Helmholtz corrections. When $\kappa = 10^{-3}$ ($\kappa = 10^{-4}$), the propagation angles $|\theta| = 10°$, $20°$, $30°$ and $40°$ correspond to transverse velocities of $|V| \simeq 3.94$, 8.14, 12.91 and 18.76 ($|V| \simeq 12.47$, 25.74, 40.82 and 59.33), respectively.

Perturbed Helmholtz solitons with $0 < \sigma \leq 2$ tend to exhibit self-sustaining periodic (or very nearly periodic) oscillations in the beam parameters (amplitude, width, and area = amplitude × width). Typical behaviour found in this regime is shown in Fig. 5. Two characteristics that have emerged from our simulations are: (*i*) for fixed β, the longitudinal

period of the reshaping oscillation tends to increase as $\sigma \to 2$; (*ii*) for fixed σ, the longitudinal period decreases with increasing β. We classify these solitons as stable limit-cycle attractors of the system.[23,24,38,39]

We now analyse solitons in the conditionally-stable regime (where $2 < \sigma < 4$) in terms of the power of the input beam, denoted by $P_{\rm in}$. Typical curves in the (β, P) plane for solution (20) are shown in Fig. 3(a). The intuitive nonlinear-dynamical approach of Pelinovsky *et al.*[14] predicts that when $0 < \beta < \beta_{\rm max}$, small perturbations leading to $P_{\rm in} < P_{\rm max}$ can induce periodic oscillations. Here, the power $P_{\rm in}(\beta;V)$ of the input beam (25) is related to the power P of the unperturbed beam (i.e., the solution where $|V| = 0$ and thus $|\theta| = 0$) through[24]

$$P_{\rm in}\left(\beta;V\right) = \frac{1}{\sqrt{1+2\kappa V^2}} P\left(\beta\right) = P\left(\beta\right)\cos\theta\,. \tag{26}$$

Since $P_{\rm in}$ is always less than P, we expect to find periodic oscillations for small values of θ. The effect of arbitrarily large perturbations cannot be quantified using the analytical technique of Ref. 14, and one must resort to fully-nonlinear (computational) methods. We present specific beam reshaping results from simulations with $\sigma = 2.5$, which requires $0 < \beta < \beta_{\rm max} \simeq 1.32$. These results illustrate well the qualitative behaviour of perturbed beams for different values of σ in the range $2 < \sigma < 4$.

Small perturbations, where $P_{\rm in}$ is slightly less than P, tend to induce long-term periodic oscillations in the beam parameters [see Fig. 6(a)], in agreement with Ref. 14. Larger perturbations, where $P_{\rm in}$ is strongly reduced by increasing θ, can lead to instability: the beam undergoes diffractive spreading, tending asymptotically toward a flat state characterized by zero amplitude and infinite width. Simulations have revealed that the solitons are most robust when β is sufficiently less than $\beta_{\rm max}$, and that the required perturbation magnitude for diffractive instability is lowered as $\beta \to \beta_{\rm max}$. This effect is shown in Fig. 6 – as the size of the perturbation increases, the instability appears sooner in part (b), where the value of $\beta = 1.0$ is closer to $\beta_{\rm max}$ than the value $\beta = 0.4$ in part (a).

3.3. $\sigma \geq 4$ *instability*

The VK criterion predicts that paraxial solutions are unstable for $\sigma \geq 4$. Previously,[14] this instability was reported as beams suffering catastrophic self-focusing (a "blow-up" phenomenon) in finite ζ, in which the beam width collapses toward zero size and the peak amplitude increases rapidly.[19] This type of singular behaviour is usually interpreted as an artefact of the SVEA.[41,42] Here, we explore the nature of this instability and uncover that the exact solution can play a key role as a boundary between qualitatively distinct beam instabilities.

We consider launching perturbed on-axis beams of the form

$$u(\xi,0)=\eta\left[A\cosh\left(\frac{\sigma\sqrt{2\beta}}{a}\xi\right)+1\right]^{-1/\sigma}. \tag{27}$$

The ratio of the energy-flows of initial condition (27) and exact soliton (9) is simply $W_{\text{in}}/W = a$, where W is given by Eqs. (18*a*) and (18*d*). The perturbation is thus parameterized by a, which controls the amount of power in the input beam. When $a = 1$ (i.e., where the initial condition is an exact solution) and in the absence of any perturbations, one may expect that the beam would propagate indefinitely and with no change to its shape.

Figure 7 compares numerical predictions, made in the vicinity of $a = 1$, when employing the classic split-step method[25,43] (to integrate the corresponding paraxial equation[13]) and the Helmholtz difference-differential algorithm.[40] Both contexts lead to the same qualitative phenomena. For $a < 1$, the beam undergoes diffractive spreading, while for $a > 1$ self-focusing gives rise to beam narrowing. Exact solution (9) with $\sigma \geq 4$ may be interpreted as an unstable manifold between localized nonlinear-wave states that undergo either narrowing or diffractive spreading (depending on whether the input power is less or greater than that of the exact solution). Figure 7 also illustrates that a tiny amount of numerical noise is sufficient for an otherwise exact solution to eventually lose stability. The Helmholtz and paraxial solutions exhibit the same type of initial qualitative behaviour for any given a, while good

quantitative agreement between these solutions is found over longer simulation lengths when $a < 1$.

4. Conclusion

We have derived two novel families of exact analytical solitons of a Helmholtz equation whose nonlinearity is of the purely focusing generalized cubic-quintic type. The spatial symmetry of both forward- and backward-propagating beams has been explored in detail. New conservation laws have been reported and it has been shown that, by integration of the governing equation, one can arrive at a very general representation of Helmholtz-bright-soliton conserved quantities [i.e., Eqs. (18*a*)–(18*e*)]. The nature of the paraxial approximation has been discussed in terms of a simultaneous algebraic multiple limit, and we have also shown that the backward solutions have no analogue in the corresponding NLS model.[13]

We have further shown that by exploiting spatial symmetry, conventional semi-analytical methods may be used in combination with computer simulations to study the stability properties of the new Helmholtz solitons. In general, they can be robust against perturbations to their shape, in the sense that they can be classified as limit-cycle attractors. An analysis of solutions in unstable regimes has also been carried out. Exact solution (9) with $\sigma \geq 4$ provides a boundary between sub-critical and super-critical beams that suffer diffractive collapse and narrowing due to self-focusing, respectively. In sub-critical regimes ($a < 1$), Helmholtz and paraxial solutions behave almost identically; in the super-critical regime ($a > 1$), both solutions undergo narrowing. These effects are of interest in the context of universal amplitude equations involving Helmholtz-type generalizations of the linear wave operator. However, higher-order nonparaxial effects would need to be incorporated to investigate the consequences of narrowing due to self-focusing of optical beams.

The results presented in this paper, along with those of Refs. 23 and 24, provide a fairly comprehensive overview of how Helmholtz solitons behave in materials with a dual power-law refractive index. Between the three papers, we have analysed a wide range of (bright)

hyperbolic and (bright and dark) algebraic solitons, as well as boundary solitons and periodic waves. This range of new solutions spans three parameter combinations for the nonlinear coefficients n_σ and $n_{2\sigma}$ in model (1). The remaining choice, where $n_{2\sigma} < 0$ and $n_{2\sigma} < 0$, is of the purely defocusing type and hence cannot be expected to support bright-type solutions (nor do we expect to find dark-type solutions for arbitrary σ).

Our analyses are of fundamental physical importance, opening up the possibility of modelling beam multiplexing[9] and interface[10–12] applications in a much wider range of optical media. Advances in materials fabrication methods and refractive-index patterning techniques mean that in the foreseeable future, waveguide architectures with application-specific (n_σ, $n_{2\sigma}$), as well as tailored values of σ, may well be within reach. Helmholtz soliton theory is also of intrinsic mathematical appeal; for instance, it maps out the structure and properties of exact soliton solutions to generic nonintegrable elliptic equations. This paper concludes our interest in the dual power-law problem (at least so far as deriving nonlinear basis functions goes), and we close by reiterating that the Helmholtz modelling approach could play a key role in the design of future nonlinear-photonic devices that involve arbitrary-angle effects.

References

1. G. I. Stegeman and M. Segev, *Science* **286**, 1518 (1999).
2. Y. S. Kivshar, *Opt. Quantum Electron*. **30**, 571 (1998).
3. Y. S. Kivshar and B. Luther-Davies, *Phys. Rep.* **298**, 81 (1998).
4. V. E. Zakharov and A. B. Shabat, *Sov. Phys.* JETP **34**, 62 (1972).
5. J. P. Gordon, *Opt. Lett.* **8**, 596 (1983).
6. O. Cohen, R. Uzdin, T. Carmon, J. W. Fleischer, M. Segev, and S. Odouov, *Phys. Rev. Lett.* **89**, 133901 (2002).
7. A. B. Aceves, J. V. Moloney, and A. C. Newell, *Phys. Rev.* A **39**, 1809 (1989).
8. A. B. Aceves, J. V. Moloney, and A. C. Newell, *Phys. Rev.* A **39**, 1828 (1989).
9. P. Chamorro-Posada and G. S. McDonald, *Phys. Rev.* E **74**, 036609 (2006).
10. J. Sánchez-Curto, P. Chamorro-Posada, and G. S. McDonald, *Opt. Lett.* **35**, 1347 (2010).
11. J. Sánchez-Curto, P. Chamorro-Posada, and G. S. McDonald, *J. Opt.* A: Pure Appl. Opt. **11**, 054015 (2009).
12. J. Sánchez-Curto, P. Chamorro-Posada, and G. S. McDonald, *Opt. Lett.* **32**, 1126 (2007).
13. R. W. Micallef, V. V. Afansjev, Y. S. Kivshar, and J. D. Love, *Phys. Rev.* E **54**, 2936 (1996).
14. D. E. Pelinovsky, V. V. Afansjev, and Y. S. Kivshar, *Phys. Rev.* E **53**, 1940 (1996).
15. K. Hayata and M. Koshiba, *Phys. Rev.* E **51**, 1499 (1995).
16. N. Akhmediev, A. Ankiewicz, and R. Grimshaw, *Phys. Rev.* E **59**, 6088 (1999).
17. A. Biswas, *Opt. Commun.* **235**, 183 (2004).
18. D. Mihalache, M. Bertolotti, and C. Sibilia, *Progress in Optics* **27**, 229 (1989).
19. A. W. Snyder and D. J. Mitchell, *Opt. Lett.* **18**, 101 (1993).
20. K. I. Pushkarov, D. I. Pushkarov, and I. V. Tomov, *Opt. Quantum Electron.* **11**, 471 (1979).

21. K. Hayata and M. Koshiba, *J. Opt. Soc. Am.* **11**, 2581 (1994).

22. D. E. Pelinovsky, and Y. S. Kivshar, and V. V. Afansjev, *Phys. Rev.* E **54**, 2015 (1996).

23. J. M. Christian, G. S. McDonald, and P. Chamorro-Posada, *J. Phys*. A: *Math. and Theor.* **40**, 1545 (2007).

24. J. M. Christian, G. S. McDonald, and P. Chamorro-Posada, *J. Phys.* A*: Math. and Theor.* **43**, 085212 (2010).

25. M. D. Feit and J. A. Fleck, *J. Opt. Soc. Am. B* **5**, 633 (1988).

26. A. P. Sheppard and M. Haelterman, *Opt. Lett.* **23**, 1820 (1998).

27. T. A. Laine and A. T. Friberg, *J. Opt. Soc. Am.* B **17**, 751 (2000).

28. P. Chamorro-Posada, G. S. McDonald, and G. H. C. New, *J. Opt. Soc. Am.* B **19**, 1216 (2002).

29. P. Chamorro-Posada, J. Sánchez-Curto, V. E. Grikurov, G. S. McDonald, and J. M. Christian, *Helmholtz solitons: Maxwell's equations, interfaces, bistability, & counterpropagation – Proceedings of the International Conference* "*Days on Diffraction*," St. Petersburg, Russia (June 2008) pp. 28–33.

30. M. Lax, W. H. Louisell, W. B. McKnight, *Phys. Rev.* A **11**, 1365 (1975).

31. S. Chi and Q. Guo, *Opt. Lett.* **20**, 1598 (1995),

32. B. Crosignani, A. Yariv, and S. Mookherjea, *Opt. Lett.* **29**, 1254 (2004).

33. A. Ciattoni, B. Crosignani, S. Mookherjea, and A. Yariv, *Opt. Lett.* **30**, 516 (2005).

34. P. Chamorro-Posada, G. S. McDonald, and G. H. C. New, *J. Mod. Opt.* **47**, 1877 (2000).

35. H. Goldstein, *Classical Mechanics* 2nd Ed. (Philippines: Addison-Wesley, 1980).

36. M. G. Vakhitov and A. A. Kolokolov, *Radiophys. Quantum Electron*. **16**, 783 (1973).

37. E. W. Laedke, K. H. Spatschek, and L. Stenflo, *J. Math. Phys.* **24**, 2764 (1983).

38. J. M. Christian, G. S. McDonald, and P. Chamorro-Posada, *J. Opt. Soc. Am.* B **26**, 2323 (2009).

39. J. M. Christian, G. S. McDonald, and P. Chamorro-Posada, *Phys. Rev.* A **76**, 033833 (2007).

40. P. Chamorro-Posada, G. S. McDonald, and G. H. C. New, *Opt. Commun.* **192**, 1 (2001).

41. E. W. Laedke and K. H. Spatschek, *Phys. Lett.* A **74**, 205 (1979).

42. Y. V. Katyshev, N. V. Makhaldiani, and V. G. Makhankov, *Phys. Lett.* A **66**, 456 (1978).

43. T. R. Taha and M. J. Ablowitz, *J. Comp. Phys.* **55**, 203 (1984).

Figure Captions

Fig. 1. Schematic diagram illustrating the geometry of (a) forward and (b) backward beams in the laboratory (unscaled) frame. Under a reversal of the coordinate axes (the space inversion operation, $x \rightarrow -x$ and $z \rightarrow -z$), the forward beam is transformed into the backward beam and vice-versa.

Fig. 2. Schematic diagram (to scale) showing typical (a) paraxial ($\theta = +2°$) and (b) arbitrary ($\theta = +60°$) propagation angles in the laboratory frame. If the transverse beam width is Λ_0 then the projected beam width at angle θ is $\Lambda_\theta = \Lambda_0 \sec\theta$. (c) Geometrical broadening in Helmholtz soliton (9) with $\sigma = 1.4$ and $\beta = 1.0$ for a range of propagation angles. Other parameters: $\alpha = \gamma = 1$.

Fig. 3. (a) Beam power P as a function of β for four values of σ, calculated from Eq. (18*d*). (b) Regions of stability in the (σ, β) parameter plane. Stable solitons [those satisfying the VK criterion (23)] lie below the curve $\beta_{max}(\sigma)$ (in the unshaded region), which has been determined numerically. Solutions with $0 < \sigma \leq 2$ are predicted unconditionally stable, while those with $2 < \sigma < 4$ are predicted stable provided $\beta < \beta_{max}$ (conditional stability). Solitons with $\sigma \geq 4$ are always unstable. Other parameters: $\alpha = \gamma = +1$.

Fig. 4. Spatial symmetry combined with conventional analyses can be used to predict the stability properties of Helmholtz solitons. (a) A stable quasi-paraxial beam [$\kappa << O(1)$ and $\kappa\beta << O(1)$] in an on-axis configuration in the laboratory frame. (b) A rotation of the observer's coordinate axes must not change the stability of the beam in any way (i.e., this transformation cannot induce an instability). (c) Rotating the coordinate axes through an arbitrary angle $-\theta$ [part (b)] is equivalent to rotating the beam through angle $+\theta$. If the beam in part (a) is stable, then so is the same beam in any off-axis configuration [part (c)].

Fig. 5. Evolution of the peak amplitude $|u|_m$ when the input beam is described by initial condition (24). The parameters are $\beta = 1.0$, (a) $\sigma = 1.2$ and (b) $\sigma = 1.8$. Solid line (blue): $|\theta| = 10°$; dashed line (green): $|\theta| = 20°$; dotted line (black): $|\theta| = 30°$; dot-dashed line (red): $|\theta| = 40°$.

Fig. 6. Evolution of the peak amplitude $|u|_m$ when the input beam is described by initial condition (24). The parameters are $\sigma = 2.5$, (a) $\beta = 0.4$, and (b) $\beta = 1.0$. The VK criterion is satisfied so long as $\beta < \beta_{max} \approx 1.32$. Solid line (blue): $|\theta| = 10°$; dashed line (green): $|\theta| = 20°$; dotted line (black): $|\theta| = 30°$; dot-dashed line (red): $|\theta| = 40°$.

Fig. 7. Beam evolution with $\beta = 0.5$ and $\sigma = 4.2$ for (a) Helmholtz ($\kappa = 10^{-3}$) and (b) paraxial solutions. The launched beams (27) have $a = 0.9999$ (sub-critical – solid blue line), $a = 1.0000$ (exact solution – dashed green line), and $a = 1.0001$ (super-critical – dotted black line). Both solutions exhibit the same qualitative behaviour.

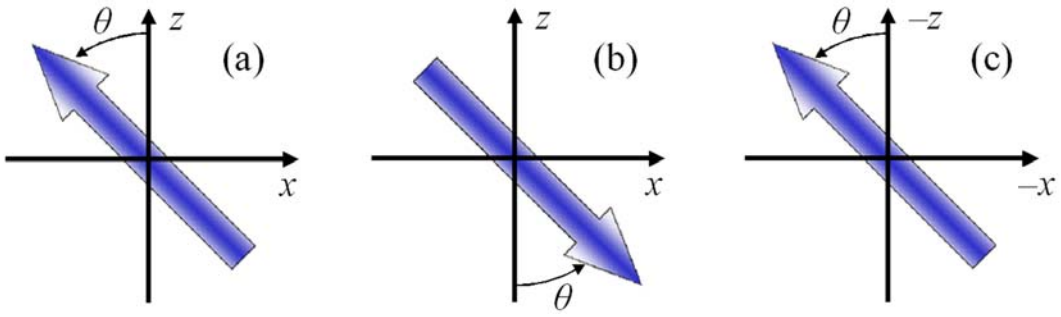

J. M. Christian, G. S. McDonald, P. Chamorro-Posada

Helmholtz solitons in optical materials with a dual power-law refractive index

Fig. 1.

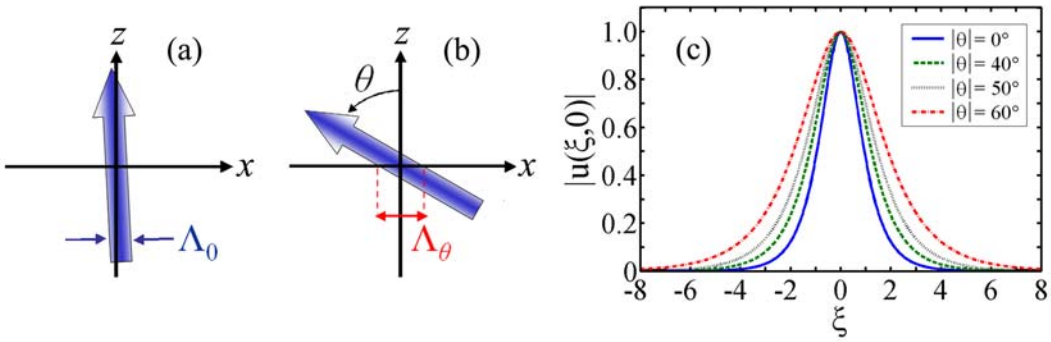

J. M. Christian, G. S. McDonald, P. Chamorro-Posada

Helmholtz solitons in optical materials with a dual power-law refractive index

Fig. 2.

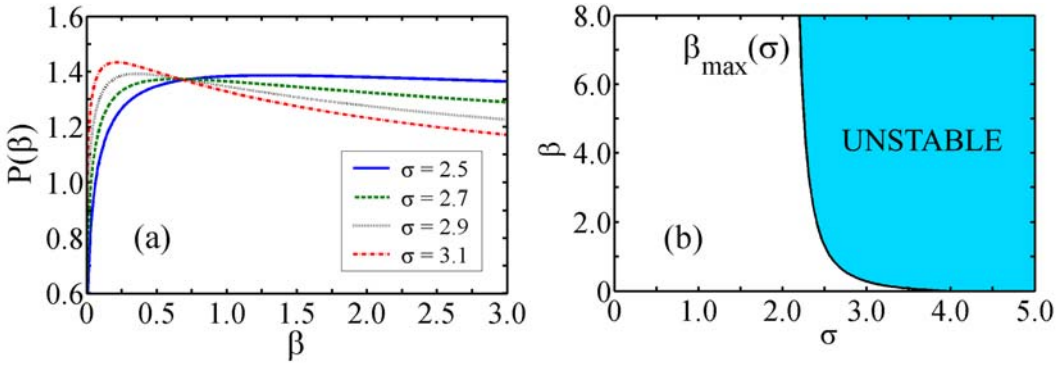

J. M. Christian, G. S. McDonald, P. Chamorro-Posada

Helmholtz solitons in optical materials with a dual power-law refractive index

Fig. 3.

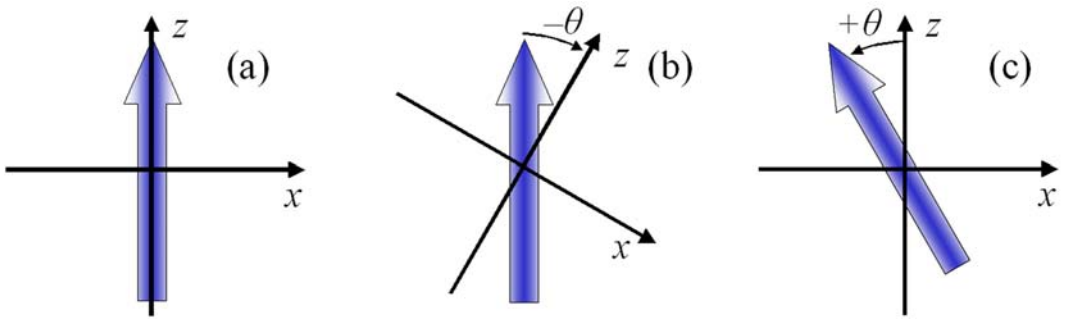

J. M. Christian, G. S. McDonald, P. Chamorro-Posada

Helmholtz solitons in optical materials with a dual power-law refractive index

Fig. 4.

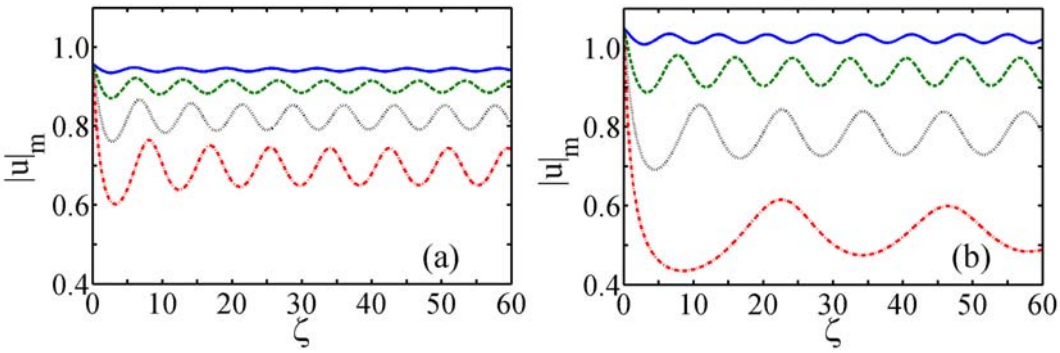

J. M. Christian, G. S. McDonald, P. Chamorro-Posada

Helmholtz solitons in optical materials with a dual power-law refractive index

Fig. 5.

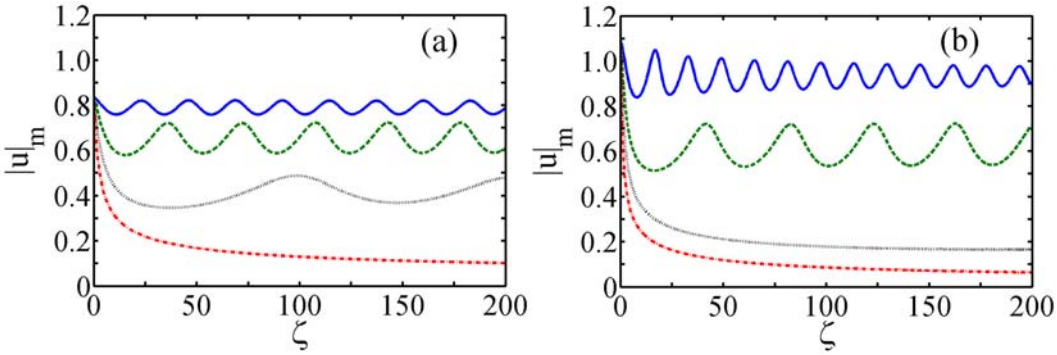

J. M. Christian, G. S. McDonald, P. Chamorro-Posada

Helmholtz solitons in optical materials with a dual power-law refractive index

Fig. 6.

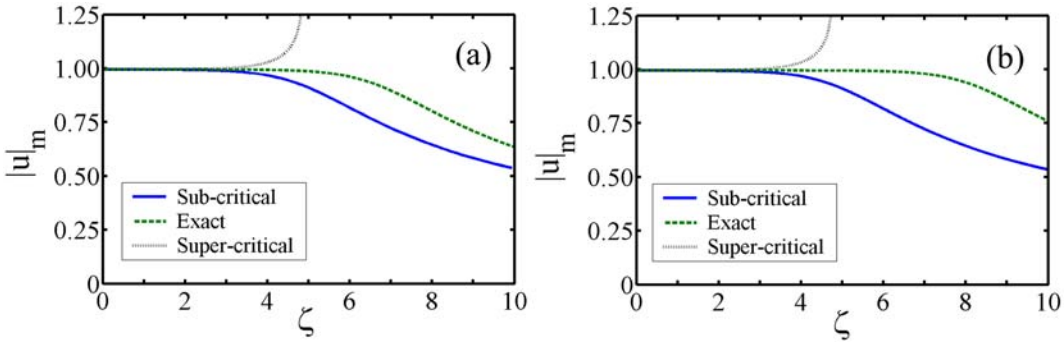

J. M. Christian, G. S. McDonald, P. Chamorro-Posada

Helmholtz solitons in optical materials with a dual power-law refractive index

Fig. 7.